Nanoscale

COMMUNICATION

View Article Online
View Journal | View Issue

Cite this: *Nanoscale*, 2025, **17**, 6466

Received 23rd January 2025,
Accepted 3rd February 2025

DOI: 10.1039/d5nr00331h

rsc.li/nanoscale

Carbon quantum dots modified with hyperbranched polyglycerol for bioapplications: improved photostability and temperature selectivity†

Shingo Sotoma, * Kota Shiraya, Suzune Shimomura, Yumi Yoshida and Kohji Maeda

There is a growing demand for technologies to accurately measure intracellular temperatures. Carbon quantum dots (CQDs) are promising candidates due to their unique properties, including high biocompatibility and ease of functionalization, attracting notable attention for applications in intracellular temperature measurements. Nevertheless, CQD-based measurements are susceptible to photobleaching and environmental factors beyond temperature (pH, ion concentration, viscosity, and biomolecules), compromising their accuracy. This study demonstrates that modifying the surface of nitrogen- and sulfur-doped CQDs (N,S-CQDs) with hyperbranched polyglycerol (HPG) mitigates the effects of surface-derived fluorescence, emphasizing core-derived fluorescence, which significantly improves their photostability and robustness against environmental changes. These HPG-modified N,S-CQDs, N,S-CQD-HPG, show reliable and repeatable temperature sensing, making them highly suitable for precise temperature measurements in complex biological environments. These findings highlight the importance of strategic surface modification in developing reliable nanometric temperature sensors for diverse applications.

With the recent advancement of nanotechnology, there is an increasing demand for temperature measurement technologies with high spatial resolution at the submicron scale. Traditional techniques such as infrared thermometry,[1,2] Raman spectroscopy,[3,4] and thin-film thermometry[5,6] lack the necessary spatial resolution to meet advanced requirements, particularly in mapping of intracellular temperature,[7] microcircuits,[8,9] and microfluidics.[10,11] In recent years, fluorescent temperature sensors have attracted attention as a technology enabling temperature measurements in the nanometric region. Various nano-sized temperature sensors have been developed, including small molecules, polymers, proteins, and metal quantum dots, which have been widely utilized in materials and biological research.[7,12] Nevertheless, there is a concern in temperature measurement at the nanoscale, as fluorescence properties can be influenced by local environmental factors. This issue is particularly critical in intracellular temperature measurements. The intracellular environment (*e.g.* pH, ions, viscosity, and biomolecules) dynamically changes in both spatial and temporal dimensions. Indeed, Baffou's group has pointed out that conventional cellular temperature sensors may be influenced by environmental factors.[13,14] Therefore, developing robust temperature sensors that can accurately measure temperature without being influenced by these factors is crucial for uncovering temperature-related cellular activities.[13,15–17]

Carbon quantum dots (CQDs) are carbon-based fluorescent nanomaterials with a size of less than ten nanometers and regarded as promising alternatives to metal-based quantum dots such as CdS and CdSe. They have attracted attention in various fields due to their biocompatibility, high dispersibility in water, ease of synthesis, surface functionality, and tunable fluorescence wavelengths.[18,19] Several studies have demonstrated that the fluorescence intensity of CQDs exhibits temperature dependency due to the thermal activation of non-radiative decay pathways, making them highly suitable for use as temperature sensors.[20] For example, Yang *et al.* reported a temperature sensitivity of −0.85% °C^{-1} within the range of 20–80 °C.[21] Liu *et al.* demonstrated that nitrogen and sulfur co-doped CQDs (N,S-CQD), which exhibit high photostability and temperature responsiveness, serve as a repeatedly used sensor with a sensitivity of −1.14% °C^{-1}.[22] To date, various types of CQDs synthesized from different precursors for use as temperature sensors have been reported and reviewed in detail elsewhere.[18,20] However, it is still challenging to use CQDs for intracellular temperature measurement because of the following issues: photobleaching and susceptibility to environmental factors beyond temperature.

To date, no method has been developed to strategically enhance both photobleaching resistance and temperature

Faculty of Molecular Chemistry and Engineering, Kyoto Institute of Technology, Kyoto 606-8585, Japan. E-mail: shsotoma@kit.ac.jp

† Electronic supplementary information (ESI) available. See DOI: https://doi.org/10.1039/d5nr00331h

selectivity. Photobleaching is the decay of fluorescence following excitation, making it difficult to distinguish changes in fluorescence intensity caused by temperature from those caused by photobleaching. Temperature selectivity here refers to the ability of a sensor to specifically respond to temperature changes without interference from environmental factors. Previous studies have addressed these issues by screening precursors.[20,23] However, such screening methods often result in unpredictable photobleaching and poor temperature selectivity. As a result, CQDs that possess both resistance to photobleaching and temperature selectivity have not been reported so far.

Here, we demonstrate that surface chemical modification enables the development of CQDs with exceptional photostability and temperature selectivity. It has been reported that there are two origins of CQD fluorescence: the aromatic sp^2 core structure and surface functional groups.[24] We found in the present work that surface-derived fluorescence is responsible for photobleaching and temperature selectivity. By eliminating surface-derived fluorescence through surface chemical modification, we successfully overcome the issues. The results underscore the importance of surface modification in overcoming the inherent limitations of CQDs and highlight the potential of these modified CQDs as robust and precise sensors for various biological and industrial applications.

For surface modification, we employed hyperbranched polyglycerol (HPG), a hydrophilic polymer with a branched structure obtained by ring-opening polymerization of glycidol.[25,26] While the HPG modification of non-doped CQDs has been previously reported,[27] the synthesis of HPG-modified N,S-CQDs has not been reported. This study aims to address this gap by exploring the enhanced properties of N,S-CQDs through HPG modification. Fig. 1a illustrates the synthetic scheme for HPG-modified CQDs. N,S-CQDs were synthesized by reacting citric acid and thiourea through a hydrothermal process. Subsequently, N,S-CQDs were reacted with glycidol, affording HPG-modified N,S-CQDs (N,S-CQD-HPG). Fig. 1b shows images of the samples under daylight and UV light. Both samples appear transparent under daylight but exhibit blue fluorescence under UV light.

To confirm the synthesis of N,S-CQD-HPG, we performed Fourier Transform Infrared (FT-IR) spectroscopy and X-ray Photoelectron Spectroscopy (XPS). Fig. 1c shows the FT-IR spectra of the samples. Strong absorption peaks at ~2800 cm^{-1} (CH_2) and ~1070 cm^{-1} (C–O–C) were observed in the N,S-CQD-HPG spectrum, attributed to the HPG coating. On the other hand, peaks at 1600–1700 cm^{-1} (C═O from carboxylic acid, ester, and/or amide) decreased significantly after HPG modification. The survey XPS spectra of the samples are displayed in Fig. 1d. In the spectrum of N,S-CQDs, peaks corresponding to C 1s, O 1s, N 1s, and S 2p are observed. However, N 1s and S 2p peaks are significantly reduced in the spectrum of N,S-CQD-HPG. XPS measures the bonding state near the material surface; thus, the reduction in N and S signal intensities in N,S-CQD-HPG indicates the existence of HPG on the CQD surface. The C 1s spectra of N,S-CQD-HPG can be deconvoluted into three peaks centered at 283.9, 285.8, and 287.6 eV, corresponding to C–C/C–O, C–S/C–N, and C═O, respectively (Fig. 1e). The peak intensities for C═O and C–S/C–N were reduced in N,S-CQD-HPG. Similarly, the O 1s spectra demonstrated that the COOH component was also reduced by the HPG coating (Fig. 1f). These results confirm the successful synthesis of N,S-CQD-HPG.

We evaluated the optical properties of N,S-CQD-HPG. Fig. 2a and b present the 2D excitation–emission map. There is moderate broadening in both the absorption and emission spectra of N,S-CQD-HPG compared to those of the N,S-CQDs, as well as a slight difference in the wavelengths of the absorption and emission maxima. Fig. 2c displays the emission, excitation, and UV-Vis absorption spectra of the samples. No marked differences are observed in the excitation and emission spectra; however, a significant difference is noted in the UV-Vis absorption spectra. In the N,S-CQD spectrum, peaks originating from the $\pi \rightarrow \pi^*$ transition at 240 nm and the $n \rightarrow \pi^*$ transition at 330 nm are identified. These peaks are attributed to the sp^2 conjugation of the aromatic ring in the core and the functional groups on the surface of CQDs, respectively.[24] In contrast, the N,S-CQD-HPG spectrum shows a decrease in the peaks associated with the $n \rightarrow \pi^*$ transition. The result indicates a substantial reduction in surface-derived emission and a predominance of core emission for N,S-CQD-HPG. This change is likely due to the consumption of surface functional groups by the ring-opening polymerization of HPG.

We examined the photostability of the samples. The relative change in fluorescence intensity was plotted against time during the excitation in Fig. 2d. As a control, we examined the photostability of N-doped CQDs (N-CQDs), which exhibit low photostability.[28] The fluorescence intensity of N-CQDs decreased to 46% after 1800 seconds, indicating photobleaching. The photostability of N,S-CQDs was improved, retaining 82% of their fluorescence intensity after irradiation. This aligns with previous reports indicating enhanced photostability through doping with multiple elements, specifically N and S in this case.[29,30] However, the observed photobleaching seriously affects the result when performing accurate temperature measurements within 1 °C. In contrast, the relative fluorescence intensity of N,S-CQD-HPG after irradiation was 97%, which represents a significant improvement in photostability compared to N,S-CQDs. Moreover, this high stability is retained under vigorous conditions, including 90 °C, 1 M NaCl, pH 3, and pH 11 (Fig. S1†). It is well known that the fluorescence of metal quantum dots is highly stable and primarily derived from the core with almost no surface-derived fluorescence. The photostability of N,S-CQD-HPG can be attributed to the disappearance of fluorescence from the surface after HPG modification, leading to an increased contribution of core fluorescence with higher photostability.

To gain further insight into the mechanism of CQD fluorescence, we measured the fluorescence lifetime and quantum yield. Fig. 2e shows the fluorescence lifetime of the samples. The decay of the N,S-CQD sample exhibited a single component with a fluorescence lifetime of 6.6 ns. On the other hand, the decay of the N,S-CQD-HPG sample showed two components, with lifetimes of 4.0 and 15.2 ns. The results suggest

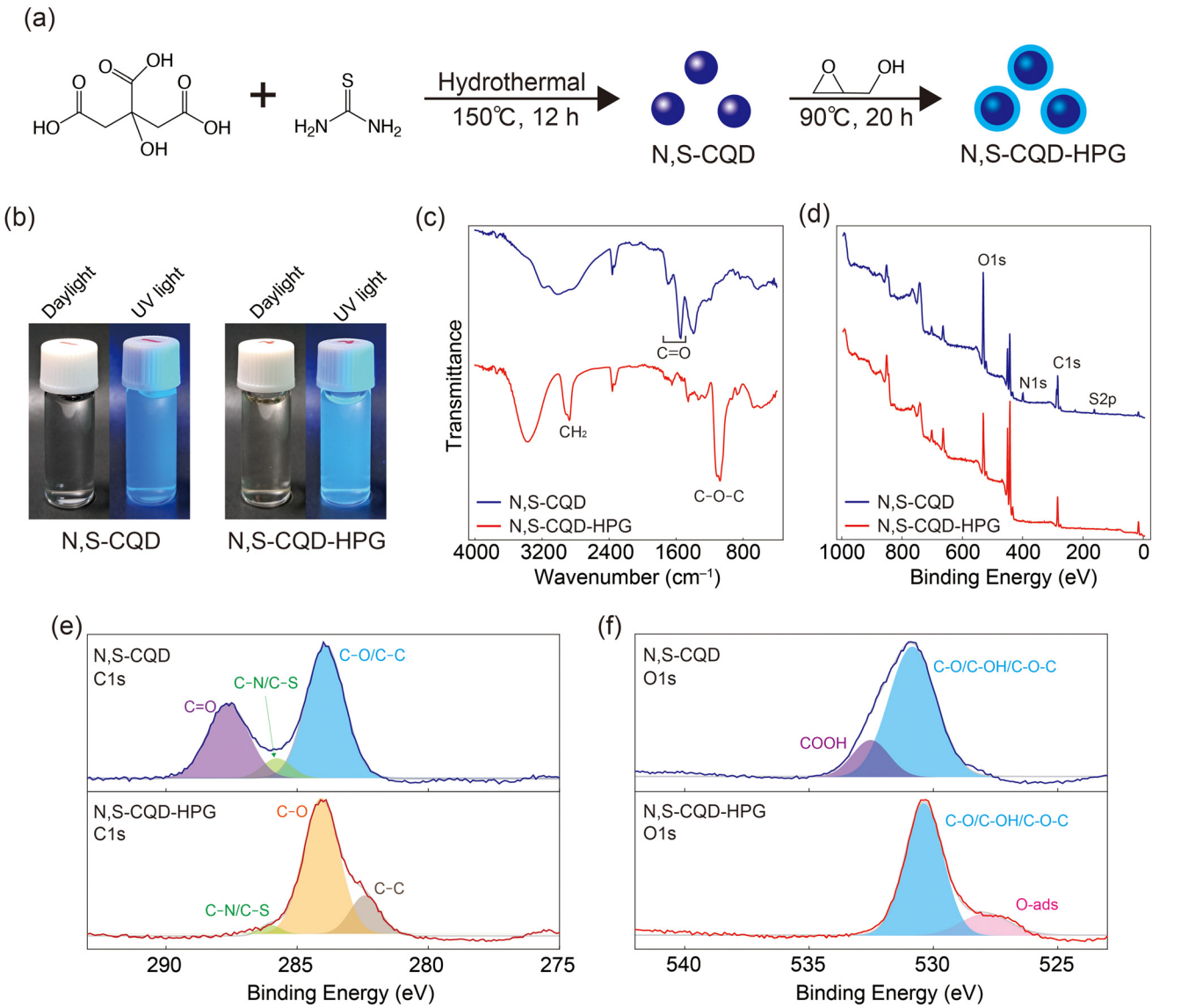

Fig. 1 (a) Schematic synthesis of N,S-CQD-HPG. (b) Images of the samples under daylight and UV light. (c) FT-IR and (d) survey XPS spectra of the samples. Deconvoluted high-resolution (e) C 1s and (f) O 1s spectra of the samples.

that the emission from the N,S-CQDs is significantly dominated by surface-originated fluorescence compared to core-originated fluorescence, whereas in N,S-CQD-HPG, the surface-originated fluorescence is attenuated, and the core-originated component becomes dominant. If this assumption is correct, there should be no significant difference in the quantum yield, but the brightness of the emission would decrease due to a reduction in the absorption cross-section. Upon measuring the quantum yield, both samples were found to have values of 29%, which is the typical value for CQDs.[31] In addition, when comparing the fluorescence intensities at the same concentration, the fluorescence intensity of N, S-CQD-HPG was reduced to about one-tenth of that of N, S-CQDs (Fig. 2f). In summary, it was confirmed that HPG modification reduces surface-originated fluorescence, which is less photostable, thereby improving the overall photostability of CQDs. It is noted that even with the fluorescence intensity reduction after HPG coating, the brightness remains sufficient for bioimaging and sensing applications.

Fig. 3a shows the temperature-dependent fluorescence spectra of N,S-CQD-HPG, which exhibit a decrease in intensity as the temperature increases. Fig. 3b displays the temperature-dependent maximum fluorescence intensity, demonstrating a linear decrease in fluorescence intensity over the range of 25–60 °C. The sensitivity was approximately −0.6% °C^{-1}, with an accuracy of ±0.9 °C at 25 °C. Note that N,S-CQDs could not be used as a temperature sensor because their fluorescence shows photobleaching with repeated irradiation, making it difficult to distinguish temperature-induced changes from those caused by photobleaching (Fig. S2†). Fig. 3c presents the results of repeated temperature measurements conducted five times between 25 and 60 °C. The result indicates that N,

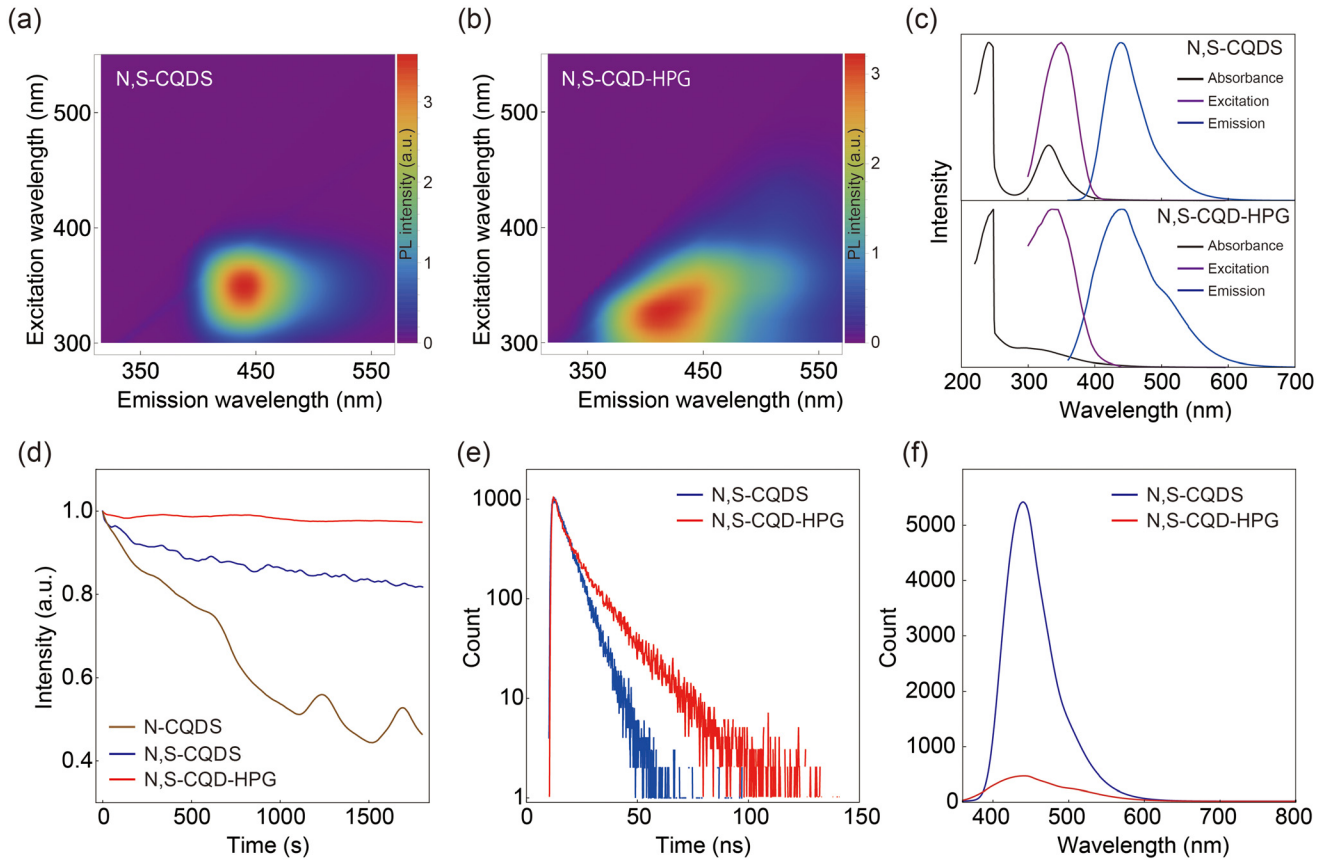

Fig. 2 Excitation–emission 2D intensity maps of (a) N,S-CQDs and (b) N,S-CQD-HPG. (c) Normalized UV-vis absorption, maximum excitation and emission spectra of the samples. (d) Relative changes in the fluorescence intensity of N-CQDs, N,S-CQDs, and N,S-CQD-HPG under excitation at 350 nm every 10 seconds. (e) Fluorescence decay of the samples in water at a temperature of 25 °C. Ex: 340 nm. (f) Fluorescence spectrum of the samples at a concentration of 10 μg ml^{-1}. Ex: 360 nm for N,S-CQDs and 340 nm for N,S-CQD-HPG.

S-CQD-HPG functions as a stable temperature sensor, allowing for consistent and reproducible measurements.

Finally, we report that HPG coating significantly reduces the environmental effects of salt concentration, pH, viscosity, and protein concentration on the fluorescence intensity of CQDs (Fig. 3d–g). For salt concentration, N,S-CQDs exhibited a fluorescence reduction of 3.5% at 100 mM and 7.7% at 1000 mM, whereas N,S-CQD-HPG showed no marked change. In terms of pH, N,S-CQDs were stable in the range of 5–9, whereas N,S-CQD-HPG was stable in the range of 3–10. Regarding viscosity, no effect on the fluorescence intensity of N,S-CQD-HPG was observed at concentrations up to 20 wt%, whereas N,S-CQDs showed a 12% enhancement at a 10 wt% glycerol concentration. For BSA concentration, N,S-CQDs demonstrated significant changes: a 7.3% enhancement of the fluorescence signal at 100 μg ml^{-1} and a 61% enhancement at 1000 μg ml^{-1}. In contrast, N,S-CQD-HPG exhibited negligible changes even at 1000 μg ml^{-1}. We also confirmed that the influence of Fe^{3+} ions, which strongly affect CQD fluorescence, is reduced in N,S-CQD-HPG (Fig. S3†). Collectively, we demonstrate for the first time that surface chemical modification, rather than precursor selection, significantly enhances photostability and temperature selectivity.

Discussion

The proposed mechanism underlying the enhanced temperature selectivity of N,S-CQD-HPG fluorescence is discussed below (Fig. 4a). The fluorescence of CQDs comprises two components: a core sp^2 aromatic ring and surface functional groups. The surface functional groups include mainly COOH from citric acid and NH_2 from thiourea, both having a lone pair of electrons contributing to the surface fluorescence, which is characterized by an n → π* transition. In NaCl aqueous solutions, these functional groups become coordinated by counter ions (Na^+ and Cl^-), leading to a perturbation of the fluorescence signal (Fig. 3d). Regarding pH, the protonation of functional groups impacts the fluorescence of CQDs. Indeed, the fluorescence of N,S-CQDs is affected at pH around 4–5 and 9–10 (Fig. 3e), which are close to the pK_a values of COOH and NH_2, respectively. We assume that the coordination and protonation are suppressed in N,S-CQD-HPG due to the HPG modification of surface functional groups, resulting in mitigated effects from salt and pH changes.

Distinct from the effects of salt and pH, N,S-CQD fluorescence was enhanced by viscosity and proteins (Fig. 3f and

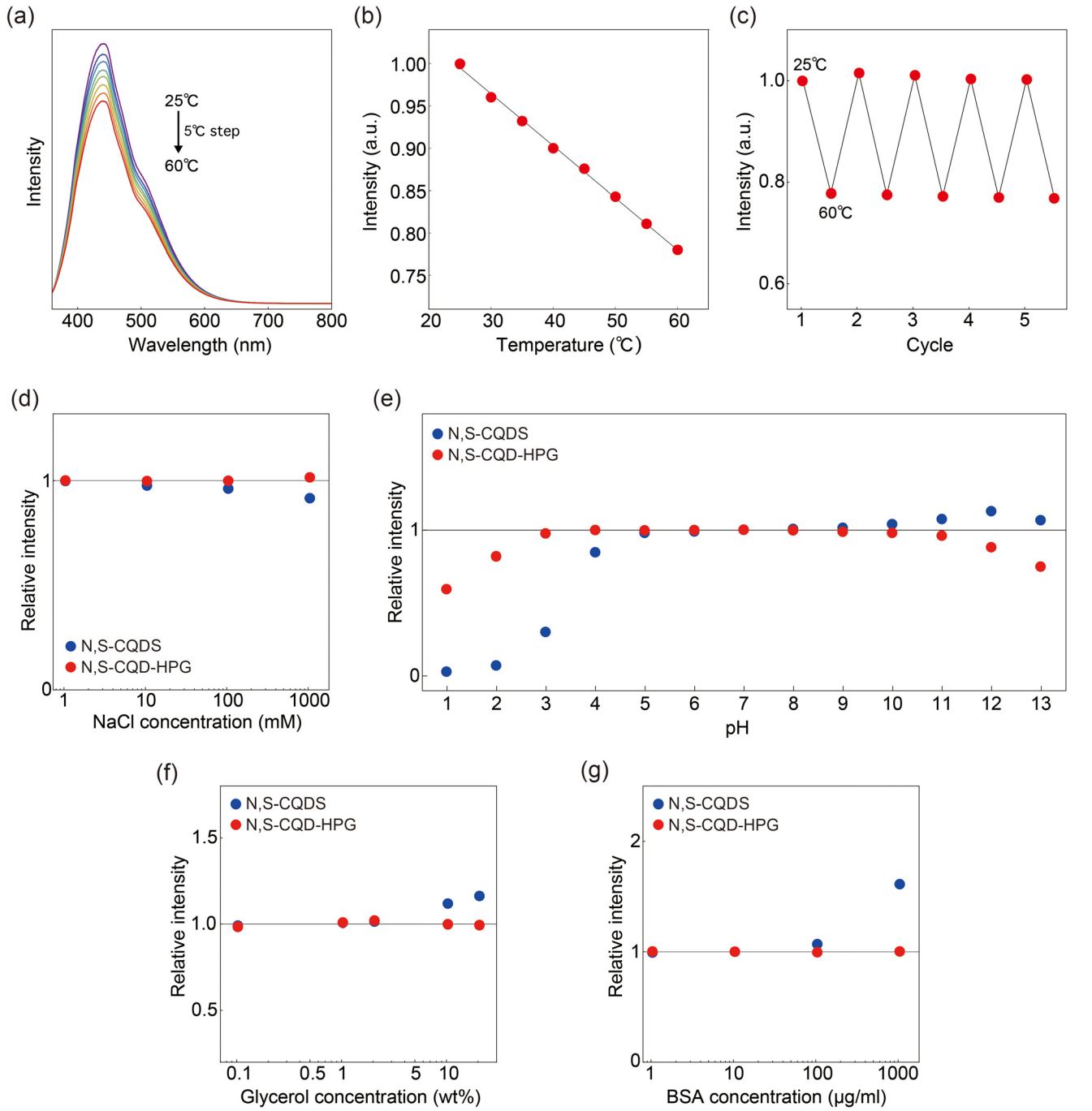

Fig. 3 (a) Temperature dependence of the fluorescence spectra of N,S-CQD-HPG in the range of 25–60 °C. (b) Fluorescence emission intensity at 450 nm as a function of temperature. (c) Fluorescence intensity change upon cycling between 25 and 60 °C for 5 cycles. (d–g) Fluorescence stability test against the environmental factors. Normalized fluorescence intensity of N,S-CQDs and N,S-CQD-HPG in (d) NaCl solution with concentrations ranging from 1 to 100 mM, (e) pH values from 1 to 13, (f) glycerol concentrations from 0.1 to 20 wt%, and (g) BSA concentrations from 1 to 1000 μg ml^{-1}.

g). This enhancement could be interpreted as viscosity and protein adsorption suppressing the non-radiative relaxation process associated with the rotational motion of surface functional groups (Fig. 4a). On the other hand, the fluorescence of N,S-CQD-HPG was not affected by either of them. HPG is a molecule with a branched glycerol-like structure, which may have already created a high viscosity state around the particles. Additionally, HPG inhibits the nonspecific adsorption of biomolecules, which is known as the stealth effect.[32] Because of these effects, N,S-CQD-HPG demonstrates excellent robustness to environmental changes and functions as a sensor that can accurately measure temperature (Fig. 4b).

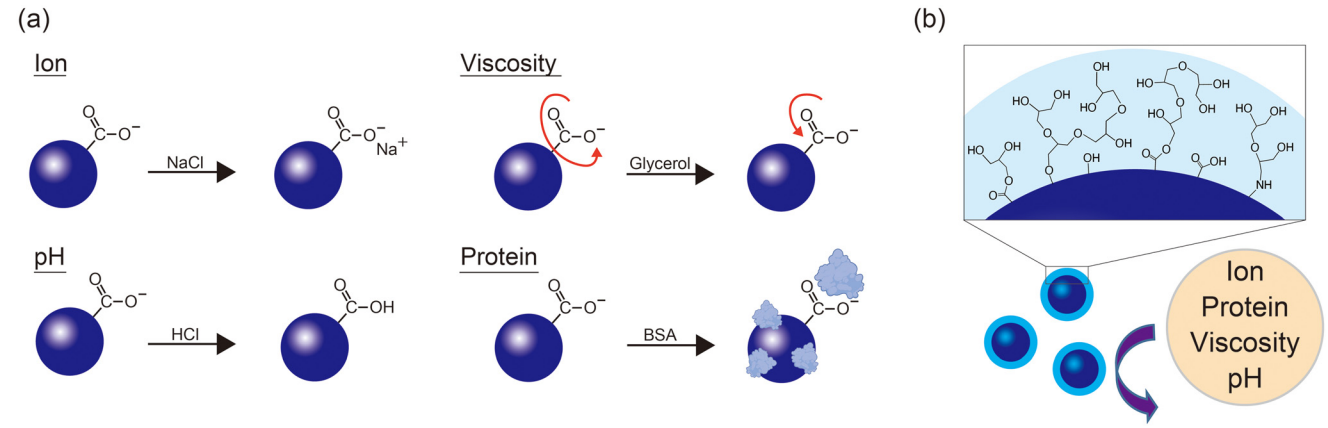

Fig. 4 (a) The mechanism by which surface-derived emission of CQDs is influenced by environmental factors. (b) Illustration of the HPG branch structure on the surface of CQDs, which suppresses the influence of environmental factors.

In summary, we investigated the effect of HPG modification on the N,S-CQD surface and its fluorescence properties. We found that HPG modification reduces the surface-derived fluorescence and dominates the core-derived fluorescence of N,S-CQDs. The loss of the surface-derived fluorescence, which is less photostable, results in increased photostability of the CQDs. This property will facilitate their long-term use. Additionally, the effects of salt, pH, viscosity, and proteins on the fluorescence were significantly reduced by a factor of 10–100, endowing the probe with high temperature selectivity for the intracellular environment.

Future efforts should focus on developing N,S-CQD-HPG with green and red emissions, as well as enhancing its sensitivity in temperature measurements. As an effective approach for addressing these challenges, the integration of machine learning techniques holds great potential.[33–36] Through these efforts, this probe is expected to play an active role in a wide range of fields from biology to industry.

Experimental

Synthesis of N,S-CQDs

420 mg of citric acid and 480 mg of thiourea were dissolved in 10 ml of Milli-Q water and placed in a 25 ml Teflon-lined stainless-steel autoclave reactor and heated at 150 °C for 12 h using an electric furnace from Nitto Kagaku. After the reaction, the solution was filtered with a membrane filter (pore size: 220 nm) to remove aggregates, dialyzed (3000 MWCO) for three hours to remove unreacted molecules and then lyophilized to obtain N,S-CQDs.

Synthesis of N,S-CQD-HPG

100 mg of N,S-CQDs was dissolved in 3 ml of glycidol, sonicated for 5 min, and stirred for 20 h at 90 °C under an argon atmosphere. After the reaction, the solution was filtered and dialyzed (1000 MWCO) for seven days to obtain N,S-CQD-HPG.

Characterization of the CQD samples

Fourier transform infrared (FT-IR) spectra of the dried samples were recorded using an FT/IR 6100 (JASCO) with a resolution of 1 cm^{-1} based on the attenuated total reflectance method. X-ray photoelectron spectroscopy (XPS) using MgKα radiation ($h\nu$ = 1253.6 eV) was performed with a JEOL 9010 X-ray photoelectron spectrometer. The samples were loaded on indium foil. UV-vis absorption spectra were collected from 220 to 600 nm using a V-630BIO (JASCO) using a 1 cm quartz cuvette. Absolute quantum yield values were measured with a Quantaurus-QY (Hamamatsu Photonics) using long neck quartz cells (1 cm optical path) and the integrated measurement software was used for the calculations. The excitation wavelength was set to 360 and 340 nm for N,S-CQDs and N,S-CQD-HPG, respectively. Photoluminescence decay curves were recorded using a lifetime spectrometer (Quantaurus-Tau, Hamamatsu Photonics) that was equipped with a 340 nm LED as a light source.

Fluorescence measurement

Fluorescence spectroscopic measurements were performed using a fluorescence spectrometer (F-8550, JASCO) equipped with a Peltier thermo-holder, which has a temperature control precision of ±0.1 °C. The sensitivity of the detector was set to medium unless otherwise specified. 2D excitation–emission fluorescence maps were recorded in an excitation range of 300–550 nm and an emission range of 315–565 nm with 5 nm and 0.5 nm slits for excitation and emission, respectively. Fluorescence stability was measured by recording the intensity of emission upon excitation every 10 seconds, which was repeated 180 times (total duration: 1800 s). As a control, nitrogen-doped carbon quantum dots (N-CQDs) synthesized from *p*-phenylenediamine were also tested.[28] These experiments were performed at 25 °C. In the experiment comparing the fluorescence intensities of N,S-CQDs and N,S-CQD-HPG, the sample concentration was set to 10 μg mL^{-1} and the sensitivity of the spectrometer's detector was set to low. Temperature-

dependent fluorescence measurements were performed in the range from 25 to 60 °C with 5 °C steps. The thermal stability was tested by repeating the 25 °C and 60 °C cycles five times. The sensitivity against temperature was calculated as the slope of the regression line. In the stability test of the environmental factors, each plot represents the relative change in the fluorescence intensity compared to that in water. Solutions with specified ionic strengths (1–1000 mM) were prepared using appropriate quantities of NaCl. The pH of each solution (pH 1.0–13.0) was adjusted using HCl or NaOH. Viscosity was modified by varying the glycerol concentration (0.1–20 wt%). Protein concentration was controlled using BSA (1–1000 μg ml^{-1}).

Author contributions

S. SO.: conceptualization, writing – original draft, writing – review & editing, methodology, and investigation, K. S.: investigation, S. SH.: investigation, Y. Y.: writing – review & editing, and K. M.: writing – review & editing.

Data availability

The data that support the findings of this study are available from the corresponding author on request.

Conflicts of interest

There are no conflicts to declare.

Acknowledgements

The authors acknowledge the financial supports from JSPS KAKENHI (19K16089 and 21K15053) and Sumitomo Research Grant (2300179).

References

1 T. Reddyhoff, H. A. Spikes and A. V. Olver, *Proc. Inst. Mech. Eng., Part J*, 2009, **223**, 1165–1177.
2 J. Nam, D.-m. Kim, M. Choi, J. Rho, J. Lee and B. J. Lee, *Infrared Phys. Technol.*, 2023, **135**, 104965.
3 S. W. Tyler, J. S. Selker, M. B. Hausner, C. E. Hatch, T. Torgersen, C. E. Thodal and S. G. Schladow, *Water Resour. Res.*, 2009, **45**, W00D23.
4 V. Zani, D. Pedron, R. Pilot and R. Signorini, *Biosensors*, 2021, **11**, 102.
5 K. G. Kreider, D. C. Ripple and W. A. Kimes, *Meas. Sci. Technol.*, 2009, **20**, 045206.
6 C. Shi, X. Wang, Q. Zheng, J. Maroske and D. Thompson, *Opt. Express*, 2024, **32**, 1003–1009.
7 K. Okabe, R. Sakaguchi, B. Shi and S. Kiyonaka, *Pflugers Arch*, 2018, **470**, 717–731.
8 P. Kolodner and J. A. Tyson, *Appl. Phys. Lett.*, 1983, **42**, 117–119.
9 W. Jung, Y. W. Kim, D. Yim and J. Y. Yoo, *Sens. Actuators, A*, 2011, **171**, 228–232.
10 H. Mao, T. Yang and P. S. Cremer, *J. Am. Chem. Soc.*, 2002, **124**, 4432–4435.
11 J. Feng, K. Tian, D. Hu, S. Wang, S. Li, Y. Zeng, Y. Li and G. Yang, *Angew. Chem., Int. Ed.*, 2011, **50**, 8072–8076.
12 J. Zhou, B. Del Rosal, D. Jaque, S. Uchiyama and D. Jin, *Nat. Methods*, 2020, **17**, 967–980.
13 G. Baffou, H. Rigneault, D. Marguet and L. Jullien, *Nat. Methods*, 2014, **11**, 899–901.
14 G. Baffou, H. Rigneault, D. Marguet and L. Jullien, *Nat. Methods*, 2015, **12**, 803.
15 Y. Takei, S. Arai, A. Murata, M. Takabayashi, K. Oyama, S. Ishiwata, S. Takeoka and M. Suzuki, *ACS Nano*, 2014, **8**, 198–206.
16 T. Sekiguchi, S. Sotoma and Y. Harada, *Biophys. Physicobiol.*, 2018, **15**, 229–234.
17 S. Sotoma, H. Okita, S. Chuma and Y. Harada, *Biophys. Physicobiol.*, 2022, **19**, e190034.
18 A. O. Adeola, A. Clermont-Paquette, A. Piekny and R. Naccache, *Nanotechnology*, 2023, **35**, 012001.
19 D. Ozyurt, M. A. Kobaisi, R. K. Hocking and B. Fox, *Carbon Trends*, 2023, **12**, 100276.
20 L. J. Mohammed and K. M. Omer, *Nanoscale Res. Lett.*, 2020, **15**, 182.
21 Y. Yang, W. Kong, H. Li, J. Liu, M. Yang, H. Huang, Y. Liu, Z. Wang, Z. Wang, T. K. Sham, J. Zhong, C. Wang, Z. Liu, S. T. Lee and Z. Kang, *ACS Appl. Mater. Interfaces*, 2015, **7**, 27324–27330.
22 G. Liu, S. Li, M. Cheng, L. Zhao, B. Zhang, Y. Gao, Y. Xu, F. Liu and G. Lu, *New J. Chem.*, 2018, **42**, 13147–13156.
23 S. Dua, P. Kumar, B. Pani, A. Kaur, M. Khanna and G. Bhatt, *RSC Adv.*, 2023, **13**, 13845–13861.
24 F. Du, L. P. Yang and L. L. Wang, *J. Mater. Chem. B*, 2023, **11**, 8117–8135.
25 L. Zhao, T. Takimoto, M. Ito, N. Kitagawa, T. Kimura and N. Komatsu, *Angew. Chem., Int. Ed.*, 2011, **50**, 1388–1392.
26 S. Sotoma and M. Shirakawa, *Chem. Lett.*, 2016, **45**, 697–699.
27 S. Li, Z. Guo, R. Feng, Y. Zhang, W. Xue and Z. Liu, *RSC Adv.*, 2017, **7**, 4975–4982.
28 K. Jiang, S. Sun, L. Zhang, Y. Lu, A. Wu, C. Cai and H. Lin, *Angew. Chem., Int. Ed.*, 2015, **54**, 5360–5363.
29 M. Yang, X. Meng, B. Li, S. Ge and Y. Lu, *J. Nanopart. Res.*, 2017, **19**, 217.
30 S. Zhu, K. Wang, J. Hu, R. Liu and H. Zhu, *Mater. Adv.*, 2020, **1**, 3176–3181.
31 A. Salvi, S. Kharbanda, P. Thakur, M. Shandilya and A. Thakur, *Carbon Trends*, 2024, **17**, 100407.
32 S. Sotoma, R. Igarashi, J. Iimura, Y. Kumiya, H. Tochio, Y. Harada and M. Shirakawa, *Chem. Lett.*, 2015, **44**, 354–356.

33 H. Guo, Y. Lu, Z. Lei, H. Bao, M. Zhang, Z. Wang, C. Guan, B. Tang, Z. Liu and L. Wang, *Nat. Commun.*, 2024, **15**, 4843.
34 Q. Xu, Y. Tang, P. Zhu, W. Zhang, Y. Zhang, O. S. Solis, T. S. Hu and J. Wang, *Nanoscale*, 2022, **14**, 13771–13778.
35 A. Döring, Y. Qiu and A. L. Rogach, *ACS Appl. Nano Mater.*, 2024, **7**, 2258–2269.
36 Q. Xu, Y. Niu, J. Li, Z. Yang, J. Gao, L. Ding, H. Ni, P. Zhu, Y. Liu, Y. Tang, Z.-P. Lv, B. Peng, T. S. Hu, H. Zhou and C. Xu, *Carbon Neutrality*, 2022, **1**, 13.